Supporting Information

In-Situ Synthesis of Bimetallic Selenides on Green Porous Carbon: Density Functional Theory-Proven Electrocatalysts for Efficient Water Splitting

Anjana Sajeevan[a], Nijash Neermunda[a], Sampath Karingula[a], Pooja[b], Soumyajit Jana[a], Ravindar Pawar[b], Yugender Goud Kotagiri[a*]

a - Department of Chemistry, Indian Institute of Technology Palakkad, Palakkad, Kerala, 678623, India

b - Department of Chemistry, Narional Institute of Technology Warangal, Hanumakonda, 506004, India,

*Corresponding authors email: yugenderkotagiri@iitpkd.ac.in

Contents

Supporting Information

1. Synthetic Protocol followed for VN synthesis

Scheme S1: Synthetic protocol followed for the synthesis of Green leaf extract, VN Extract. First, leaves were collected (1) and washed thoroughly with water to remove dust and debris. Later, it was allowed to dry in room temperature for 3 days (2). The dry leaves were grinded into fine powder using a mixer grinder (4). 50 g of the powder was added into a 1 L round bottom flask containing 450 mL of distilled water and 50 mL of methanol (4) and stirred

continuously for 12 h at 60°C to obtain VN extract (5) and was maintained at room temperature, filtered through whatman filter paper (6) to obtain a brownish liquid) used as a carbon source as well as green reducing agent (7).

2. UV-Visible Spectra of Metal ions and phytochemical reduced metal complexes

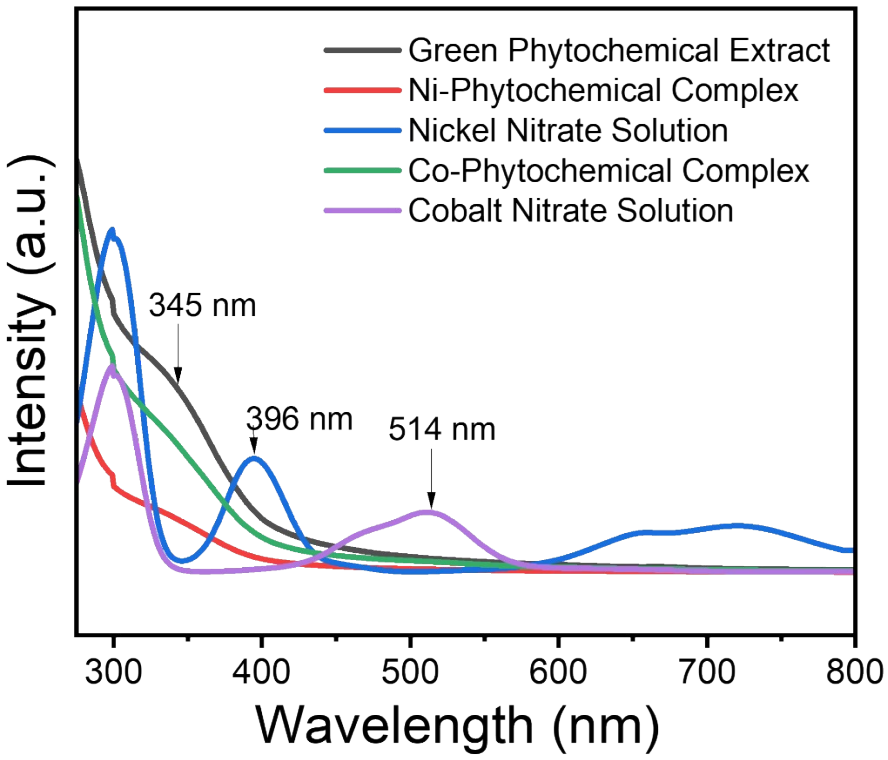

Figure S1: *UV-Visible Spectra of Green Phytochemical Extract, Nickel Nitrate solution, Cobalt Nitrate Solution, Nickel-Phytochemical Complex and Cobalt-Phytochemical Complex*

3. CHNS Elemental Analysis of GPC/$NiSe_2$/$CoSe_2$ varying amounts of VN Extract

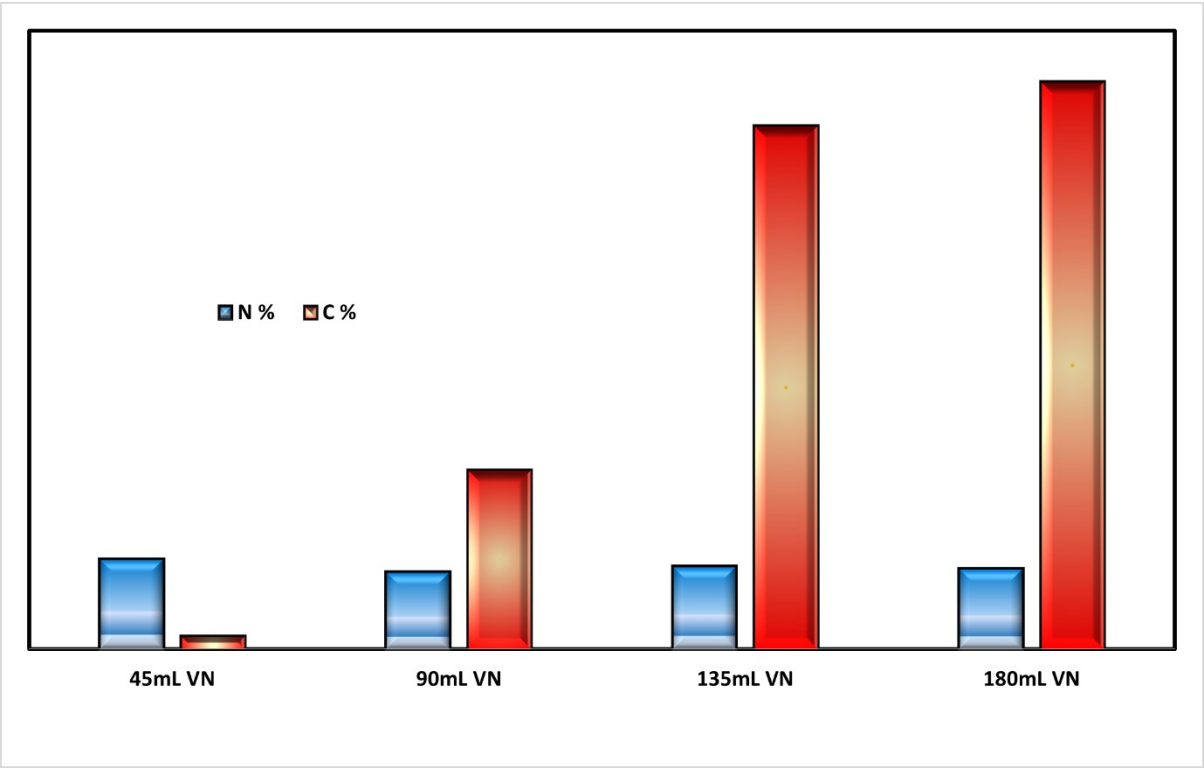

Figure S2: *CHNS Elemental Analysis of GPC/$NiSe_2$/$CoSe_2$ in varying amounts of VN*

4. XPS Survey Scan of GPC/$NiSe_2$/$CoSe_2$

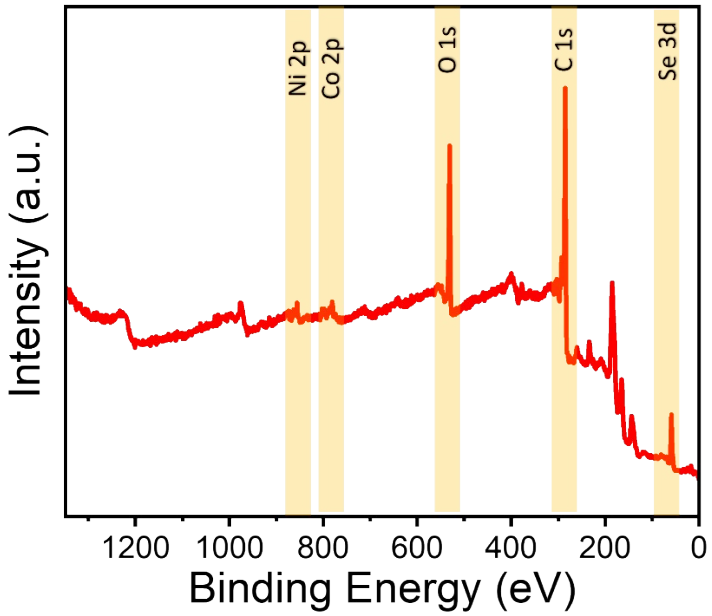

Figure S3: *Survey Scan spectrum of GPC/$NiSe_2$/$CoSe_2$ indicating the presence of Nickel, Cobalt, Selenuim and Carbon in the catalyst*

5. Deconvoluted XPS Spectrum of Se 3d

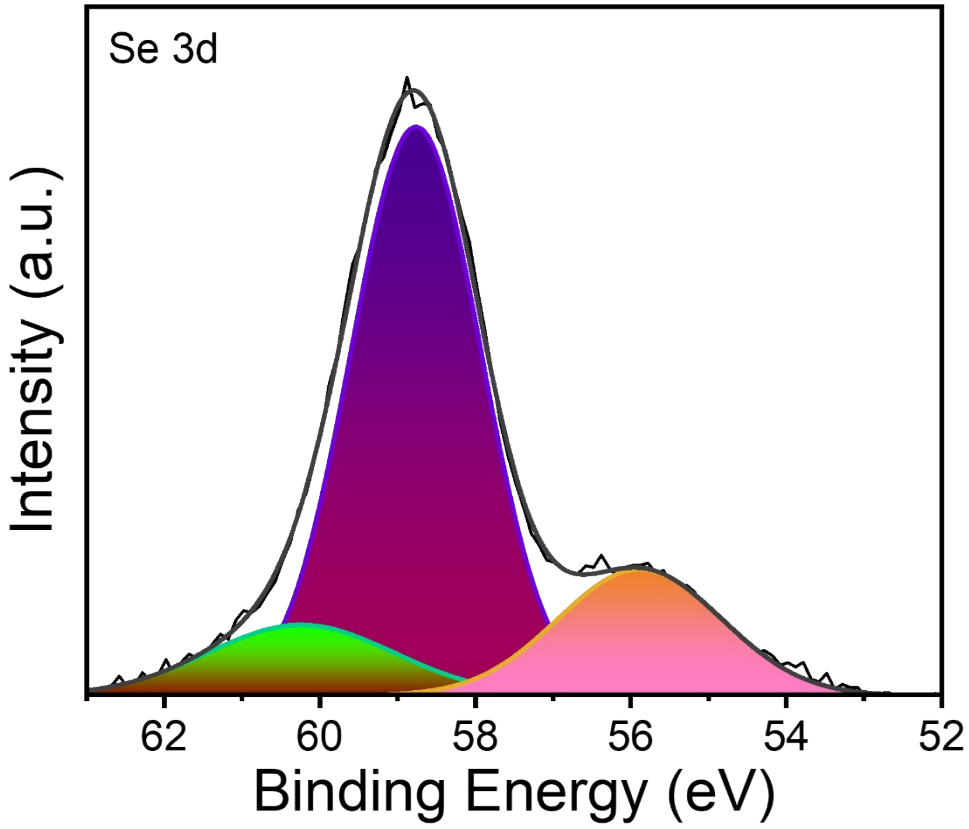

Figure S4: *Deconvoluted XPS scan of Se 3d, showing 2 major peaks, corresponding to Se $3d_{3/2}$ and Se $3d_{5/2}$ at 55.4 eV and 54.3 eV respectively. The additional peak at 58.9 eV can be attributed to the SeOx component.*

6. Post Characterization FESEM images of GPC/$NiSe_2$/$CoSe_2$

Figure S5: *Post stability FESEM images*

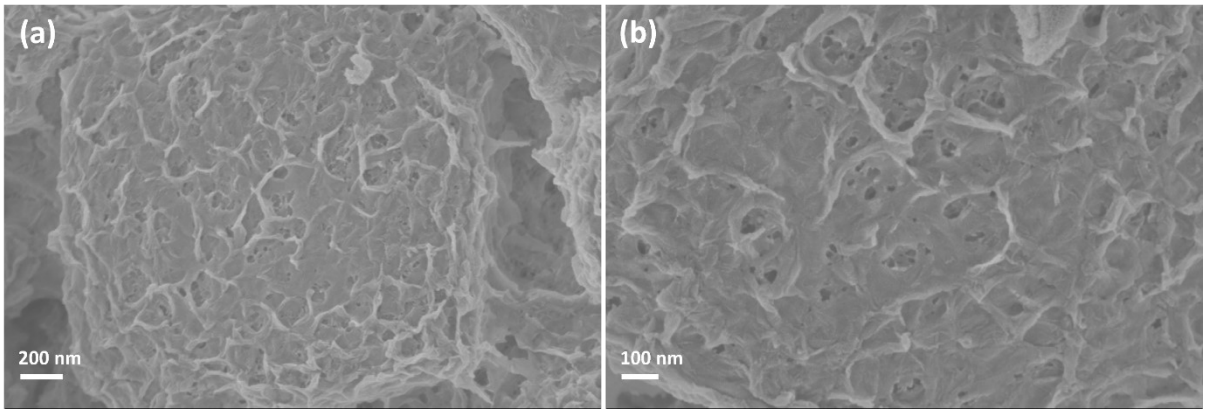

Figure S5: *FESEM images of GPC/$NiSe_2$/$CoSe_2$ after stability test in 200 nm (a) and 100 nm scale (b)*

7. BET Pore Size Distribution of GPC/NiCo

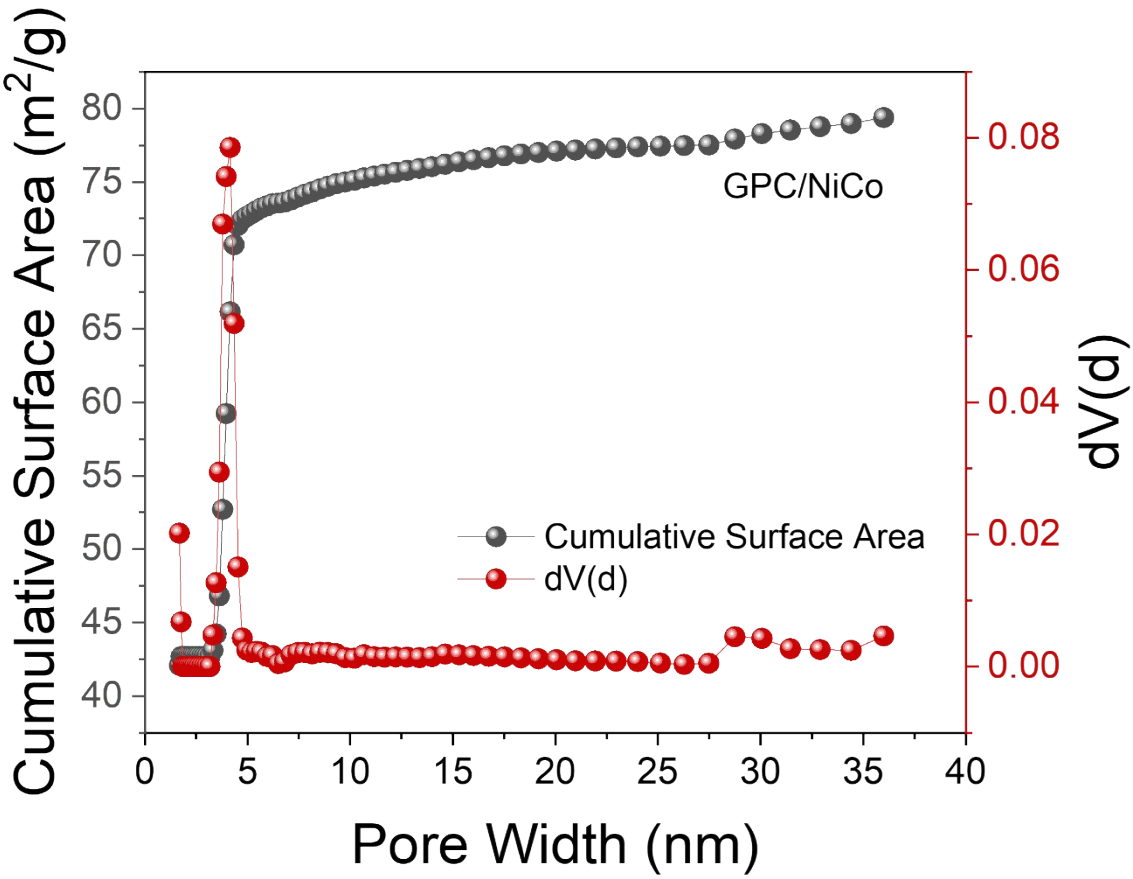

Figure S6. *BET Pore Size Distribution of GPC/NiCo, where differential pore volume is plotted against pore width*

8. BET Pore Size Distribution of GPC

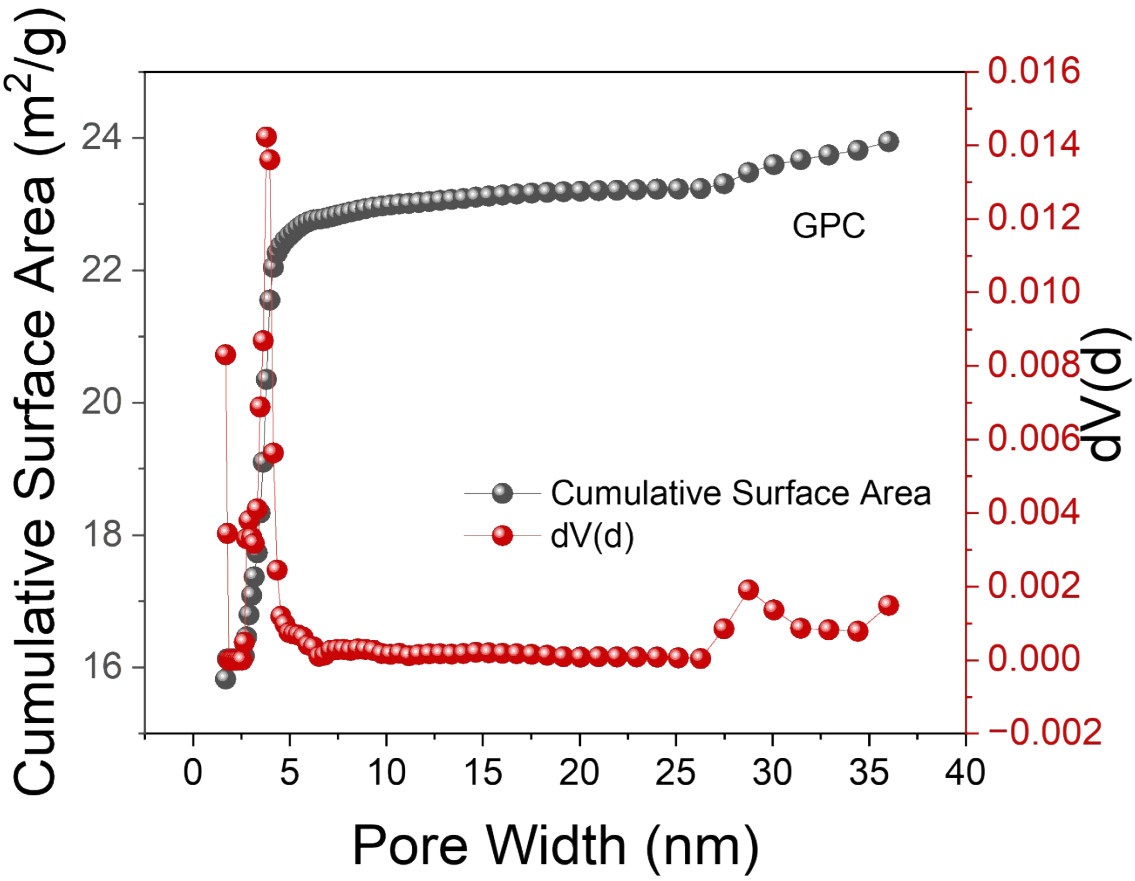

Figure S7. *BET Pore Size Distribution of GPC where differential pore volume is plotted against pore width*

9. Cyclic voltammograms of GPC, GPC/NiCo, GPC/$NiSe_2$/$CoSe_2$

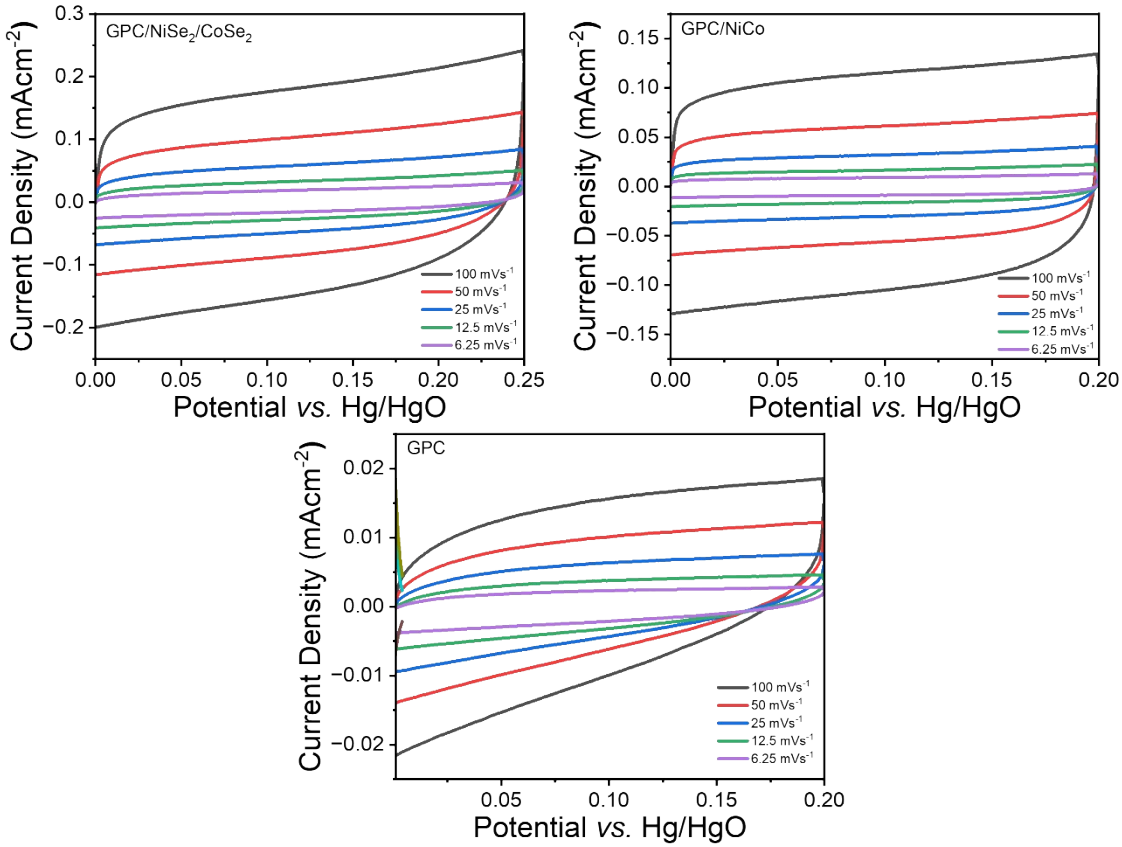

Figure S8. *Cyclic voltammograms of all the three materials GPC, GPC/NiCo, GPC/$NiSe_2$/$CoSe_2$ used to calculate double layer capacitance values*

10. Calculation of Electrochemically active Surface Area, ECSA

Electrochemical Surface area calculation: Cyclic Voltammetry was performed in different scan rates in the potential range, 0-0.2 V vs Hg/HgO. The ECSA was calculated using the formula,

ECSA = Cdl/Cs, where Cs= Specific Capacitance and Cdl= Double Layer Capacitance.

Sample	Double Layer Capacitance (mF cm^{-2})
GPC/$NiSe_2$/$CoSe_2$	3.14
GPC/NiCo	2.15
GPC	0.219

Figure S9. *Calculation of Electrochemically active Surface Area, ECSA*

11. Contact Angle measurements of GPC/NiCo and GPC

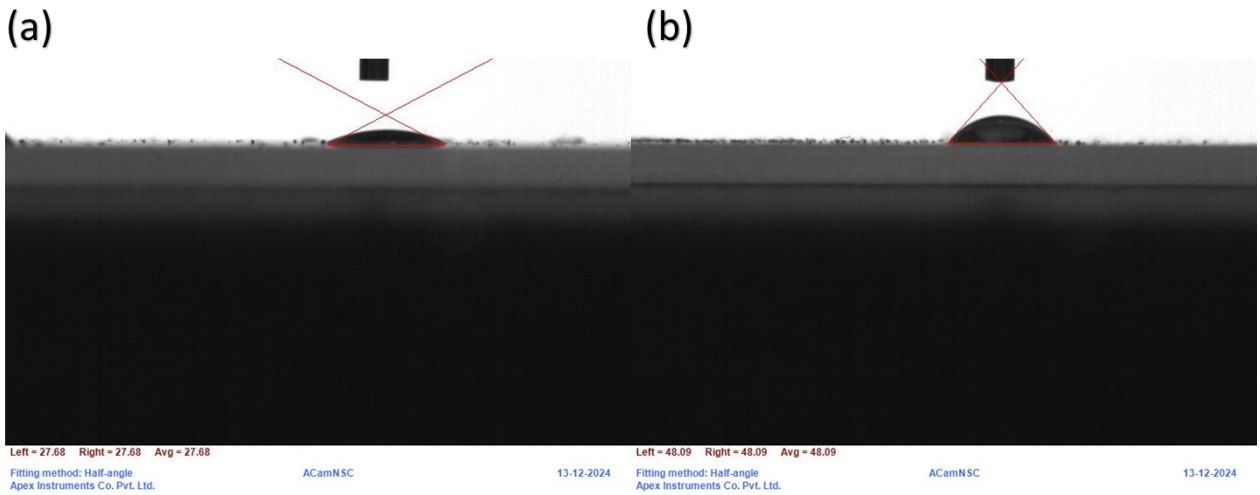

Figure S10. *Contact Angle measurements of (a) GPC/NiCo and (b) GPC using tangent method*

12. Construction of unit cell and Catalyst intermediate structures

The theoretical model was constructed to represent the carbon-supported bimetallic selenide system based on experimental observations. The crystallographic information files (CIFs) of NiSe2 and graphene were obtained from the Materials Project database. A 3 × 3 supercell was generated, with a monolayer graphene sheet placed on top of the $NiSe_2$ (2 × 2), to represent the conductive carbon layer. To account for the bimetallic composition, one Ni atom in the $NiSe_2$ lattice was substituted with a Co atom. The calculated lattice mismatch was found to be less than 1%, and a vacuum spacing of 50 Å was introduced along the z-direction to avoid interlayer interactions. Periodic boundary conditions were applied along the x- and y-directions. The elemental composition (C, Ni, Co, and Se) was guided by the atomic percentages obtained from EDS. All structures were fully optimized until the total energy convergence reached 10-5 eV and the forces were below 0.01 eV/Å.

k-point convergence tests were performed, and the 2 × 2 × 1 k-point mesh showed negligible energy changes was adopted in all calculations (Figure S19).

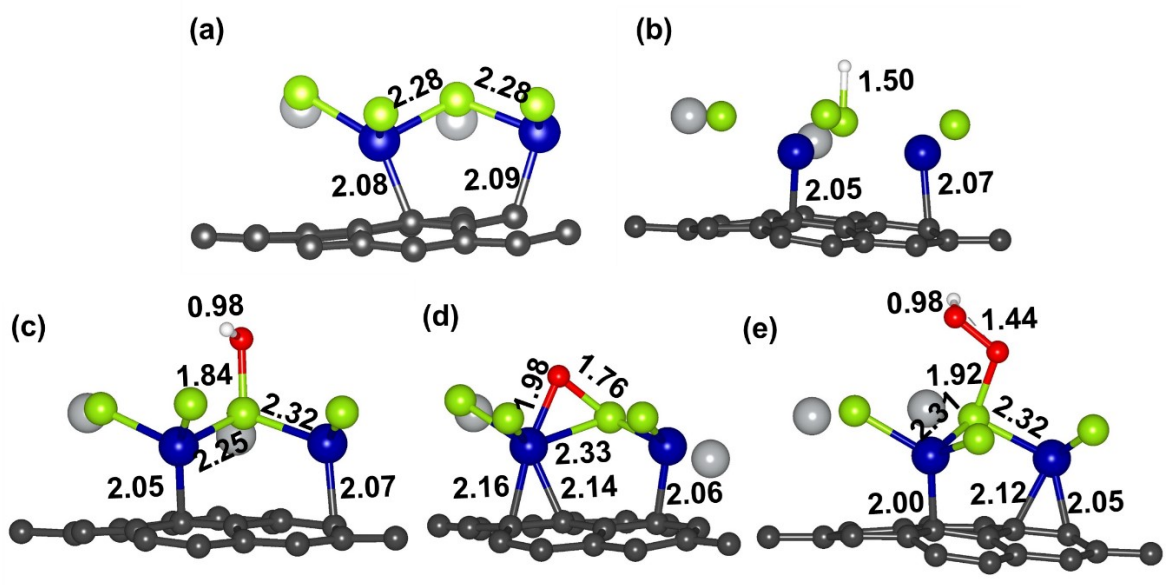

Figure S11. *Schematic representations of (a) the catalyst, intermediate structures of (b) the catalyst with H for HER, and (c) the catalyst with OH, (d) the catalyst with O, and (e) the catalyst with OOH for OER*

Colour code: Blue: Co, Green: Se, Grey: Ni, Dark Grey: C.

13. HER Catalytic Activity of GPC/$NiSe_2$/$CoSe_2$ – 45, 90, 135, 180

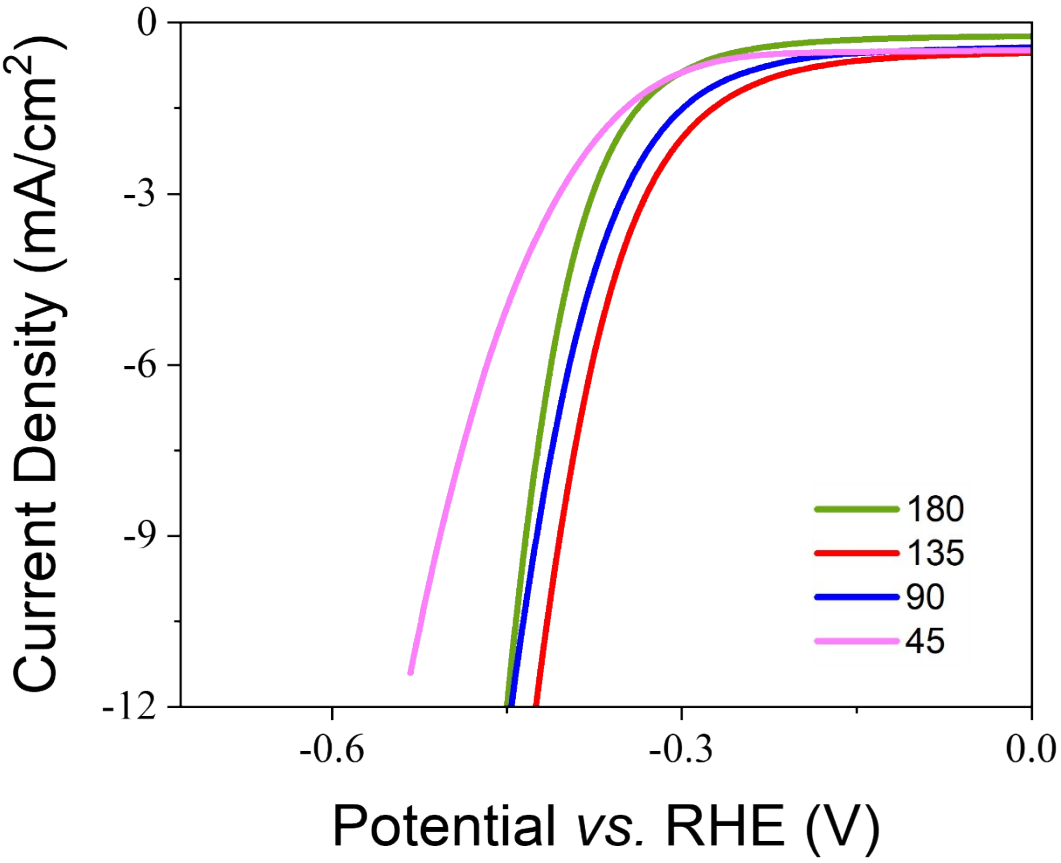

Figure S12. *HER catalytic activity of GPC/$NiSe_2$/$CoSe_2$ – 45, 90, 135, 180*

14. Nyquist Plot of GPC, GPC/NiCo and GPC/$NiSe_2$/$CoSe_2$

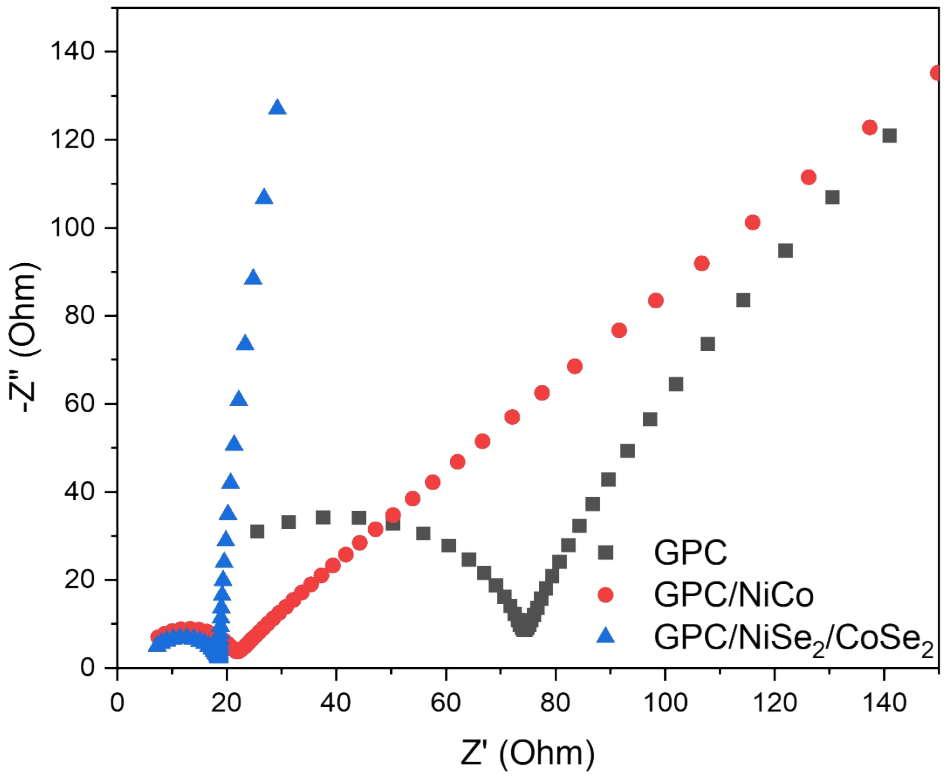

Figure S13. *Nyquist Plot of GPC, GPC/NiCo and GPC/$NiSe_2$/$CoSe_2$*

15. 1000 Cycle CV of GPC/$NiSe_2$/$CoSe_2$ for HER stability studies

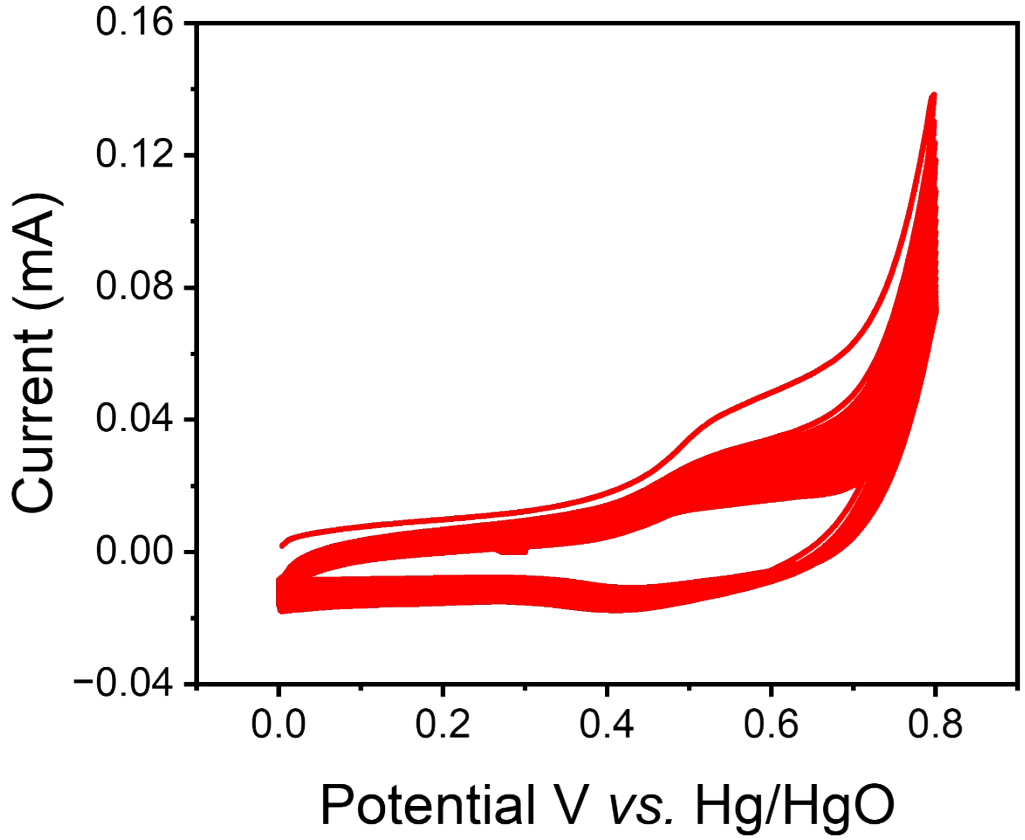

Figure S14. *1000 Cycle CV of GPC/$NiSe_2$/$CoSe_2$ for HER stability studies*

16. 1000 Cycle CV of GPC/$NiSe_2$/$CoSe_2$ for OER stability studies

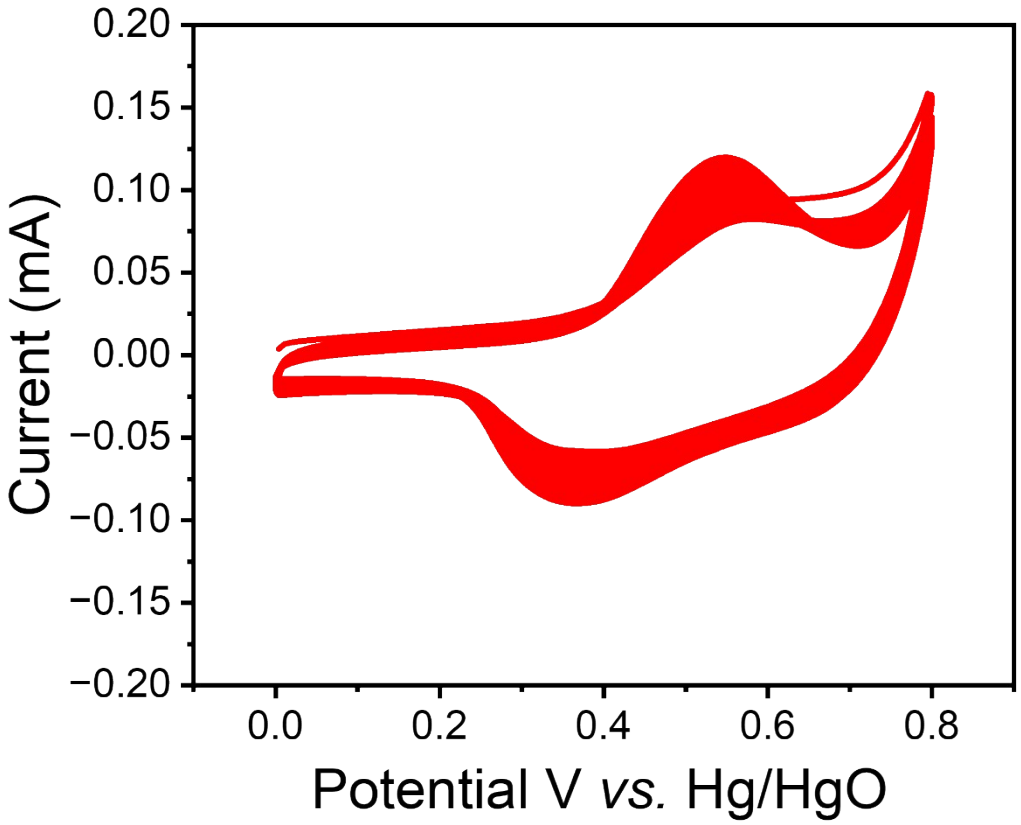

Figure S15. *1000 Cycle CV of GPC/$NiSe_2$/$CoSe_2$ for OER stability studies*

17. Comparison of HER performances of GPC/$NiSe_2$/$CoSe_2$ and $NiSe_2$/$CoSe_2$

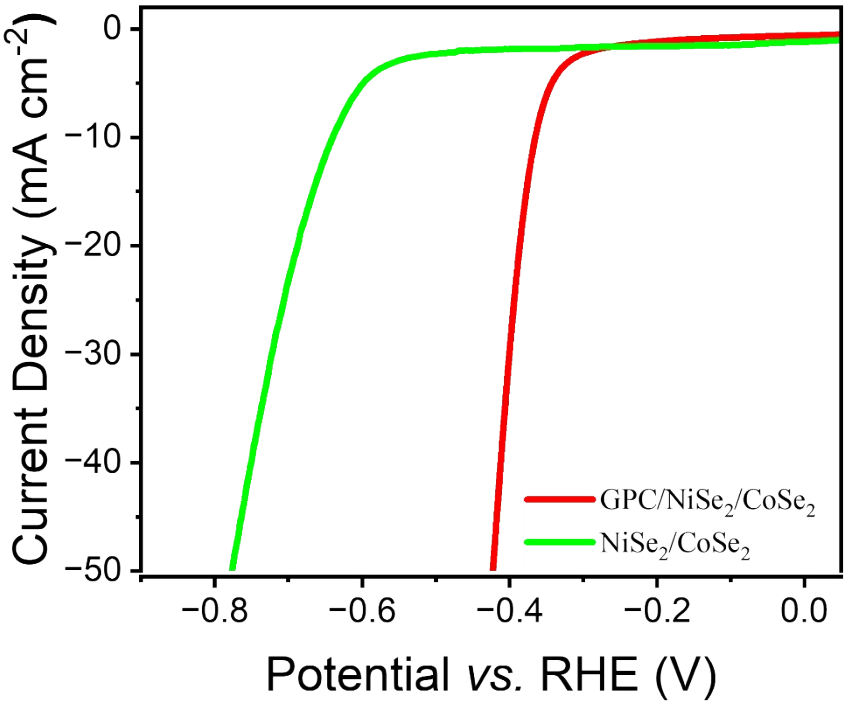

Figure S16. *Comparison of water splitting performances of GPC/$NiSe_2$/$CoSe_2$ and previously reported similar systems*

18. Comparison of HER and OER performances of GPC/$NiSe_2$/$CoSe_2$ and previously reported catalysts derived from bio-sources

Catalyst	Metals present	Tafel Slope (mV dec^{-1})		Electrolyte	Ref
		HER	OER		
Ni/NBCF-1-H_2	Ni	109	--	0.5M H_2SO_4	[1]
PSAC	--	75.7	--	0.5M H_2SO_4	[2]
NPCF	--	135	--	0.5M H_2SO_4	[3]
PBC-800	Ca	80	--	0.5M H_2SO_4	[4]
CoTBrPP@bio-C	Co	80	--	1M KOH	[5]
Co_2P-NC	Co	78	--	1M KOH	[6]
NiO_x-AC-500	Ni	121	--	0.1M KOH	[7]
Co@NPC-T*fu*	Co	--	63.9	1M KOH	[8]
$CoS_{1.097}$-B	Co	--	83	1M KOH	[9]
M_{FeMn}CNH	Fe/Mn	--	64.6	1M KOH	[10]
FeCo-NC_{ps}	Fe/Co	--	87	0.1M KOH	[11]
GPC/$NiSe_2$/$CoSe_2$	Co,Ni	72	61	0.1M KOH	This work

Figure S17. *Comparison of HER and OER performances of GPC/$NiSe_2$/$CoSe_2$ and previously reported catalysts derived from bio-sources*

19. Comparison of HER performances of GPC/$NiSe_2$/$CoSe_2$ and previously reported transition metal oxide catalysts

Catalyst	Metals present	Overpotential		Electrolyte	Ref
		HER	OER		
Cu-300	Cu	410	--	1 M H_2SO_4	12
Cu-MOF	Cu	369	--	0.5M H_2SO_4	13
Cu-Cu_2O@C	Cu	637	--	0.5M H_2SO_4	14
WO_3–CuO/rGO	Cu, W	400	--	1M KOH	4, 15
Cl^- doped CuO	Cu	400	--	1M H_2SO_4	16
CuO nanoflowers	Cu	1020	--	0.5M H_2SO_4	17
CuO-NiO@GP	Cu, Ni	762	--	0.5M H_2SO_4	18
$Cu_{0.3}Ir_{0.7}O_\delta$	Cu, Ir	--	623	0.2 M PBS	19
Fe100	Fe	--	~780	1M NaOH	20
GPC/$NiSe_2$/$CoSe_2$	Co,Ni	366	578	0.1M KOH	This work

Figure S18. *Comparison of HER performances of GPC/$NiSe_2$/$CoSe_2$ and previously reported transition metal oxide catalysts*

20. KPOINTS convergence test

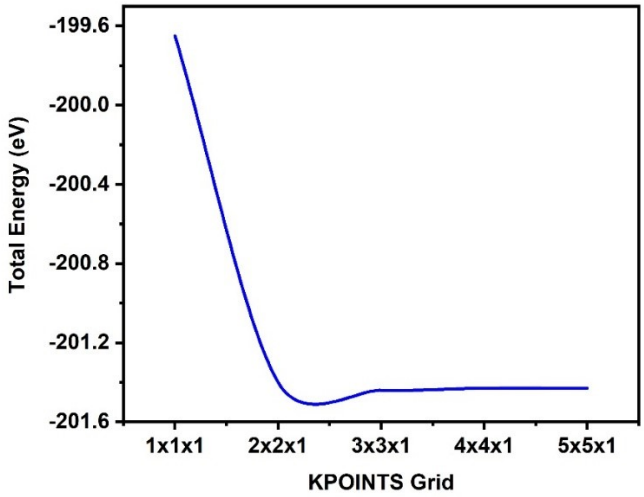

Figure S19. *k-point convergence test*

21. Cartesian Coordinates of Optimized Structures

Replaxed single unit of supercell GPC/$NiSe_2$/$CoSe_2$

1.000

7.40317242 0.00000000 0.00000000

-3.70158621 6.41133538 0.00000000

0.00000000 0.00000000 50.68503800

C Ni Se Co

18 2 4 2

Cartesian

0.00000000 0.00000000 0.17125950

1.23386207 0.71237060 0.17125950

2.46772414 0.00000000 0.17125950

4.93544828 0.00000000 0.17125950

3.70158621 0.71237060 0.17125950

6.16931035 0.71237060 0.17125950

-1.23386207 2.13711179 0.17125950

-2.46772414 4.27422359 0.17125950

0.00000000 2.84948239 0.17125950

-1.23386207 4.98659419 0.17125950

1.23386207 2.13711179 0.17125950

0.00000000 4.27422359 0.17125950

3.70158621 2.13711179 0.17125950

2.46772414 4.27422359 0.17125950

2.46772414 2.84948239 0.17125950

1.23386207 4.98659419 0.17125950

4.93544828 2.84948239 0.17125950

3.70158621 4.98659419 0.17125950

0.00000000 0.00000000 2.62475458

3.65627308 0.00000000 2.62475458

1.82813654 1.05547512 3.93713188

5.48440962 1.05547512 3.93713188

0.00000000 4.22190049 3.93713188

3.65627308 4.22190049 3.93713188

-1.82813654 3.16642537 2.62475458

1.82813654 3.16642537 2.62475458

22. Chronopotentiometry at 100mAcm^{-2}

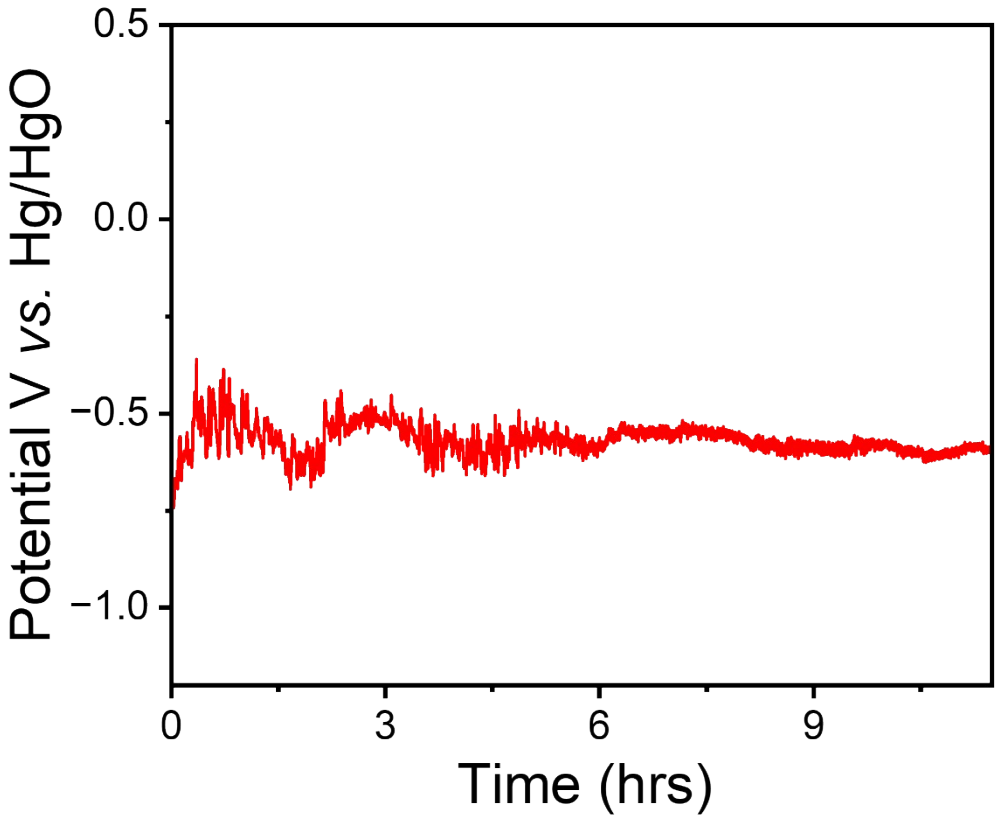

Figure S20. *12 hours long chronopotentiometry measurement of GPC/$NiSe_2$/$CoSe_2$*

References

1. S. Hong, N. Song, E. Jiang, J. Sun, G. Chen, C. Li, Y. Liu and H. Dong, *Journal of Colloids and Interface Science*, 2022, **608**, 1441-1448.
2. K. A. Saravanan, N. Prabu, M. Sasidharan and G. Maduraiveeran, *Applied Surface Science*, 2019, **489**, 725-733.
3. G. Han, M. Hu, Y. Liu, J. Gao, L. Han, S. Lu, H. Cao, X. Wu and B. Li, *Journal of Solid State Chemistry*, 2019, **274**, 207-214.
4. L. Deng, Y. Zhang, Y. Wang, H. Yuan, Y. Chen and Y. Wu, *Resources, Conservation and Recycling*, 2021, **170**, 105568.
5. X. Lv, Y. Chen, Y. Wu, H. Wang, X. Wang, C. Wei, Z. Xiao, G. Yang and J. Jiang, *Journal of Materials Chemistry A*, 2019, **7**, 27089-27098.
6. M. Yang, F. Feng, K. Wang, S. Li, X. Huang, L. Gong, L. Ma and R. Li, *ChemSusChem*, 2020, **13**, 351-359.

7. K. N. Dinh and V. G. Gomes, *Carbon*, 2020, **157**, 515-524.
8. J. Zhang, R. Z. Sun, X. F. Zhang, J. X. Wu, Y. H. Dou, X. Y. Zhu, L. H. Yu, L. Y. Guo, M. L. Liu and L. Guo, *Advanced Functional Materials*, 2022, **32**, 2202119.
9. H. Wang, F. Chang, J. Gu, X. Xie, H. Chen, Z. Bai, L. Yang and X. Yang, *International Journal of Hydrogen Energy*, 2020, **45**, 2765-2773.
10. H. Han, S. Noh, S. Chae, S. Kim, Y. Choi, T.-H. Le, M. Chang, H. Kim and H. Yoon, *Nanoscale*, 2019, **11**, 23241-23250.
11. J. Liu, T. He, Q. Wang, Z. Zhou, Y. Zhang, H. Wu, Q. Li, J. Zheng, Z. Sun and Y. Lei, *Journal of Materials Chemistry A*, 2019, **7**, 12451-12456.
12. A. Verma, P. Anand, S. Kumar and Y.-P. Fu, *Applied Surface Science*, 2022, **578**, 151795.
13. M. Jahan, Z. Liu and K. P. Loh, *Advanced Functional Materials*, 2013, **23**, 5363-5372.
14. P. Muthukumar, P. S. Kumar and S. P. Anthony, *Materials Research Express*, 2018, **6**, 025518.
15. K. M. Katubi, A.-Z. Warsi, F. Aziz, Z. A. Khattak, M. F. Warsi, M. Al-Buriahi, Z. Alrowaili and S. Yousaf, *Current Applied Physics*, 2023, **51**, 80-90.
16. D. P. Jaihindh, P. Anand, R.-S. Chen, W.-Y. Yu, M.-S. Wong and Y.-P. Fu, *Journal of Environmental Chemical Engineering*, 2023, **11**, 109852.
17. F. Naaz, A. Sharma, M. Shahazad and T. Ahmad, *ChemistrySelect*, 2022, **7**, e202201800.
18. S. B. Khan and A. M. Asiri, *Journal of Molecular Liquids*, 2021, **335**, 116084.
19. W. Sun, Y. Song, X.-Q. Gong, L.-m. Cao and J. Yang, *Chemical science*, 2015, **6**, 4993-4999.
20. M. P. Browne, S. Stafford, M. O'Brien, H. Nolan, N. C. Berner, G. S. Duesberg, P. E. Colavita and M. E. Lyons, *Journal of Materials Chemistry A*, 2016, **4**, 11397-11407.